POLYMERE SELECTIVE LASER MELTING SIMULATION USING THE C-NEM METHOD

D. Defauchy[1]*, G. Regnier[1], P. Peyre[1], I. Amran[1] and A. Ammar[2]

[1]*Arts et Métiers ParisTech, PIMM, France – denis.defauchy@ensam.eu – gilles.regnier@ensam.eu patrice.peyre@ensam.eu – amran.illoul@ensam.eu*
[2]*Arts et Métiers ParisTech, LAMPA, France – amine.ammar@ensam.eu*

Abstract - Direct manufacturing technology using Selective Laser Melting (SLM) on polymer powders allows obtaining final parts in a short time, with a high degree of flexibility concerning shapes, evolution of parts and with classical polymer density. The physical base of this process is the coalescence of grains, which initiates the densification of powder during SLM. This study will present a bi-dimensional simulation of the selective laser melting process. The C-NEM method is implemented for both hydrodynamic and thermal calculations. A particular work is done to adapt the mesh to well describe surface tension action in the vicinity of the interface. The code is validated simulating a pendant drop and basic thermal problems. The process simulation is finally presented. The degree of densification is predicted with a curvature analysis, the material thermal history is studied and the welding depth is evaluated. The characteristic times of coalescence, densification and welding are obtained. As the material has to stay melted until adding the new powder layer, good combination of parameters is determined.

Keywords: Laser, Melting, Polymer, C-NEM, Simulation.

INTRODUCTION

Polymer selective laser sintering process enables to create very light parts in a short time with complex geometries. A recent review [1] presents a good overview of the process and its difficulties. The powder densification is driven by capillary flows, whereas viscosity dissipates the energy and slows down the densification phenomenon. The coalescence phenomenon is at the origin of the densification and its kinetics has been presented in a former study [2].

Polymer powder from 20µm up to 200µm particles diameters is used. Thin layers of 100µm to 300µm are usually deposited and preheated some degrees under the material melting temperature. A laser pass melts the selected powder area to create a new slice of the final part. Coalescence, densification, welding and air diffusion [3] occurs as the material cools down and may crystallize. The material has to stay melted the longer as possible in order to obtain a good final density.
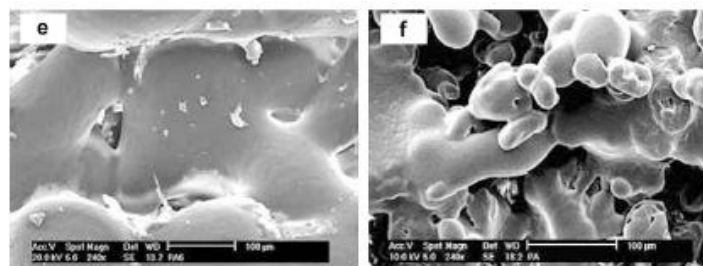

Figure 1 [4] Micrograph of PA6 (e) and PA12 (f) melted powder for same process parameters

Fig.1 presents the micrograph of PA6 and PA12 powders melted by laser sintering for the same process parameters. It is shown that the densification rate is extremely different. The quality of parts is driven by a lot of process parameters (laser power, pre-heating temperatures, laser speed, hatch distance, laser beam diameter, layer thickness, layer spreading velocity, time between layer spreading) and material parameters (viscosity, surface tension, powder geometry, thermal conductivity, heat capacity, laser absorptivity, density). Even with fixed parameters, the repeatability of parts characteristics is not easy to obtain [3] & [5].

Experimental studies are also made in order to understand the effect of each parameter and to create parts with good density and mechanical characteristics.

Simulations of the process integrating the whole local physics don't exist yet. Our first objective is to understand the role of each phenomenon and determine their kinetics. The second one is to study the influence of the process and material parameters on the densification rate, welding depth and material solid/fluid state evolution.

NUMERICAL DEVELOPMENT

Numerical method

The C-NEM method (Constrained Natural Element Method) [6,7] is based on Voronoï cells around nodes. It looks like a classical finite element method (FEM) but the shape functions (Sibson) are different. This difference permit to better take into account the participation of all nearest neighbors nodes in streams interpolations. The main advantage of this fact is that calculations are not as dependent as FEM considering distorted elements. Indeed, the mesh nodes can move with high deformation rates without remeshing properly.

The development of the method is presented in a former paper [8]. The guide lines are described here.

Hydrodynamic development

The polymer is considered as an incompressible Newtonian fluid. The basic equations which drive the fluid movements (eq.1) are integrated on the domain and the system to solve (eq.2) is introduced.

$$\begin{cases} \nabla \cdot \underline{\underline{\sigma}} + \underline{f_d} = 0 \\ \underline{\underline{\sigma}} = -p\underline{\underline{I}} + 2\mu\underline{\underline{D}} \\ div\underline{V} = 0 \end{cases} \quad (1)$$

where $\underline{\underline{\sigma}}$ is the strain tensor, $\underline{f_d}$ the volume force in the domain, $\underline{\underline{D}}$ the deformation tensor and μ the viscosity.

$$\underline{\underline{K}}\,\underline{U} = \underline{F} \quad (2)$$

where $\underline{\underline{K}}$ is the hydrodynamic matrix, $\underline{U}$ the nodal velocity and pressures and $\underline{F}$ the external surface actions vector.

The surface tension is integrated in the vector $\underline{F}$ as a pressure $\overrightarrow{P_T}$ which value is calculated (eq.3) using Laplace equation and interface equilibrium.

$$\overrightarrow{P_T} = \frac{\Gamma}{R}\vec{n} \quad (3)$$

where Γ is the material surface tension, R the local curvature ray of the interface and $\vec{n}$ the normal vector of the interface.

As the problem is discretized, R and $\vec{n}$ are evaluated with a circle adjusted to the node of the evalutaion and its two neighbors (Fig.2).
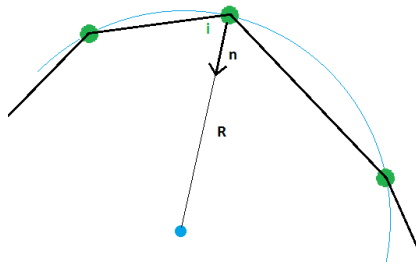

Figure 2 Discretized interface curvature ray R and normal $\vec{n}$ calculation

The velocity determination of all nodes enables to displace the nodes with a Taylor development (eq.4).

$$x(t + dt) = x(t) + v(t)dt + \gamma(t)\frac{dt^2}{2} \quad (4)$$

where $x(t)$ is the coordinates of each node at time t, v and γ its velocity and acceleration, and dt the time step.

dt is calculated at each time step using the interface nodes velocities. The criterion is an angle value ($<30°$) and the local rotation of interface segments aroud each node is limited to this value.

The viscosity is related to the temperature with an arrhenius law (eq.5).

$$\eta(T) = \eta_0(T)e^{\frac{E}{R}\left(\frac{1}{T} - \frac{1}{Tm}\right)} \quad (5)$$

where η_0 is the viscosity at melting temperature, E the activation energy, R the perfect gaz constant, T the temperature and Tm the melting temperature

Lagrangian conditions are added to take into account cavities volumes assumed as constant for SLM simulations and symmetry conditions on the domain.

Thermal development

The heat transfer equation (eq.6) is integrated on the domain and an implicit method is used to solve the system obtained. The new nodal temperature at each time step is obtained (eq.7).

$$\lambda \Delta T + P = \rho c \frac{\partial T}{\partial t} \qquad (6)$$

where λ is the thermal conductivity, P the heat source, ρ the volume mass and c the heat capacity

$$\bar{T}^{n+1} = \left[\frac{\underline{\underline{M}}}{dt} + \underline{\underline{K}}\right]^{-1} \left(\frac{\underline{\underline{M}}T^n}{dt} + \underline{B}\right) \qquad (7)$$

where T^n is the nodal temperature at time step n, $\underline{\underline{M}}$ the thermal matrix, $\underline{\underline{K}}$ the conductivity integration matrix and $\underline{B}$ the surface heat flux and volume heat flow integration vector.

The laser action is modelized by a volume heat flow $I(z)$ with a Beer-Lambert and Gaussian law (eq.8).

$$I(z) = (1 - R_e)I_0 e^{-kz} e^{-\frac{2r^2}{w^2}} \qquad (8)$$

where R_e is the material laser reflectivity, I_0 a constant depending on the laser power, k the obsorption coefficient, r the radial distance to the laser beam center, $w = \frac{R}{2.146}$ with R the laser beam diameter and z the depth in the material under laser action.

The welding quality S (eq.9) of the material is estimated regarding former work on PEEK welding study [9].

$$S = \int_{T_f}^{T_c} \frac{1}{t_r(T)} dt \qquad (9)$$

where $t_r(T) = Ae^{\frac{E}{RT}}$, $A = 7,3.10^{-6}$s and $E = 59000$ J.mol^{-1}

Meshing specifications

The C-NEM method has no meshing specifications. However, the surface tension has to be well evaluated on the nodes at the interface. Thus, it is necessary to remesh the interface and the volume in its vicinity.
An interface remeshing is performed with a local criterion in degrees per node in order to well describe the local curvature. A volume remeshing is performed, based on local mesh elements dimensions, in order to well take into account the effect of surface tension in calculations.

The code is implemented in Matlab and a validation is performed before analyzing the process.

Surface tension action

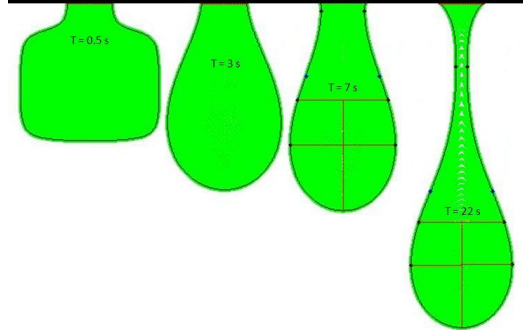The surface tension action consideration is verified simulating the bi-dimensional pendant drop (Fig.3).

Figure 3 Pendant drop simulation

Analyzing the shape evolution of the drop (V & θ - Fig.4), it is possible to calculate the surface tension initially input in the model (eq.10) studying the force equilibrium on the volume V: gravity (g) and surface tension (Γ) actions.
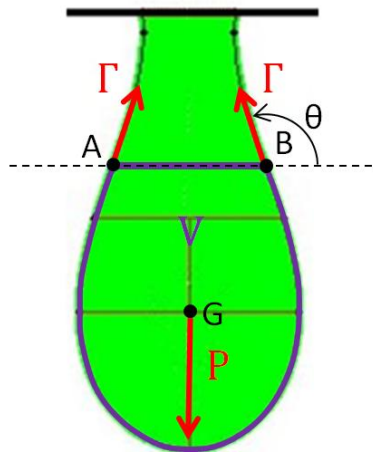
Figure 4 Pendant drop equilibrium

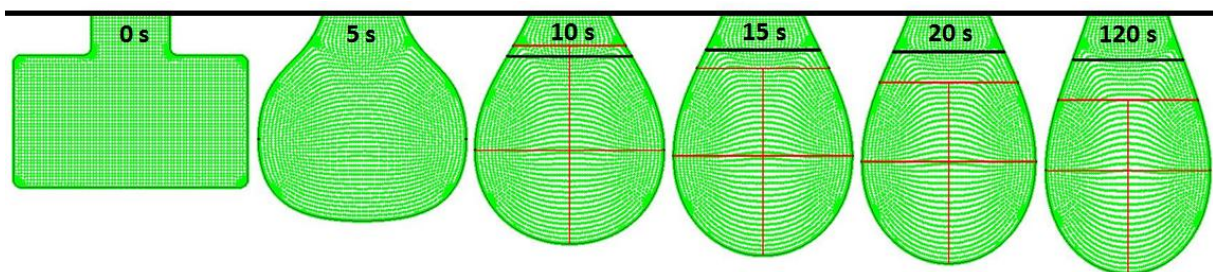$$\Gamma = \frac{\rho V g}{2 sin\theta} \qquad (10)$$

Figure 5 Pendant drop simulation

The pendant drop is simulated until its equilibrium (Fig.5) and the surface tension measurement is plotted (Fig.6).
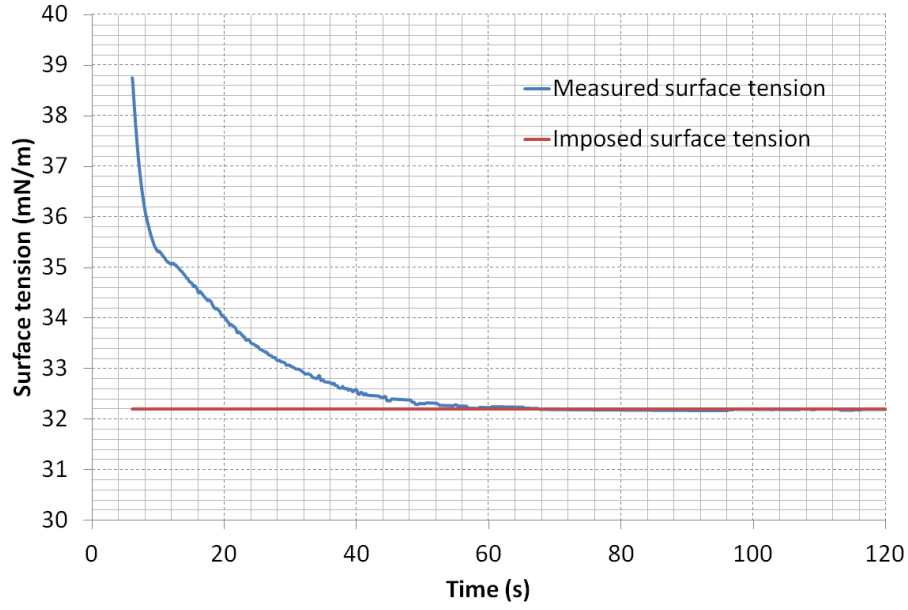
Figure 6 Surface tension measurement on pendant drop simulation

The surface tension imposed (32.2 mN.m^{-1}) is founded.

Fluid viscosity and dynamics

In order to validate the kinetics of fluids, the simulation of a cavity evolution is done regarding Kropinski [10] development. The simulation of a circular domain of fluid (R_0=100 µm) with a centered cavity (R_i=50 µm) is simulated (Fig.6). The pressure in the cavity is always equal to the external pressure. Surface tension action reduces the cavity until its closure.
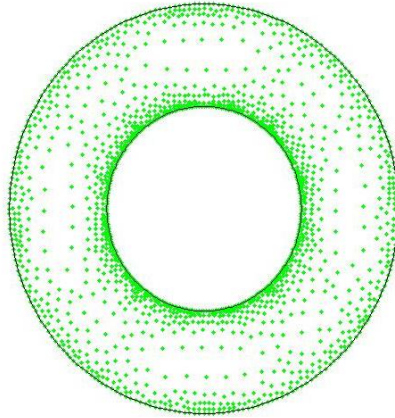

Figure 7 Initial simulation domain

The time evolutions of r_0 and r_i, external and internal ray of the domain divided by R_0 are given (eq.11 & 12) versus adimensional time τ (eq.13).

$$\tau = 2(R_i - r_i) + \sqrt{3 + 4r_i^2} - \sqrt{3 + 4R_i^2} \quad (11)$$

$$\tau = 2(r_0 - R_0) - \sqrt{4r_0^2 - 3} + \sqrt{4R_0^2 - 3} \quad (12)$$

$$\tau = t \frac{\Gamma}{\eta R_0} \quad (13)$$

The simulation is performed for a surface tension of 32.2 mN.m-1 and a viscosity of 1793 Pa.s. Simulations images are presented (Fig. 8).

t = 0s   t = 1s   t = 2s

t = 3s   t = 4s
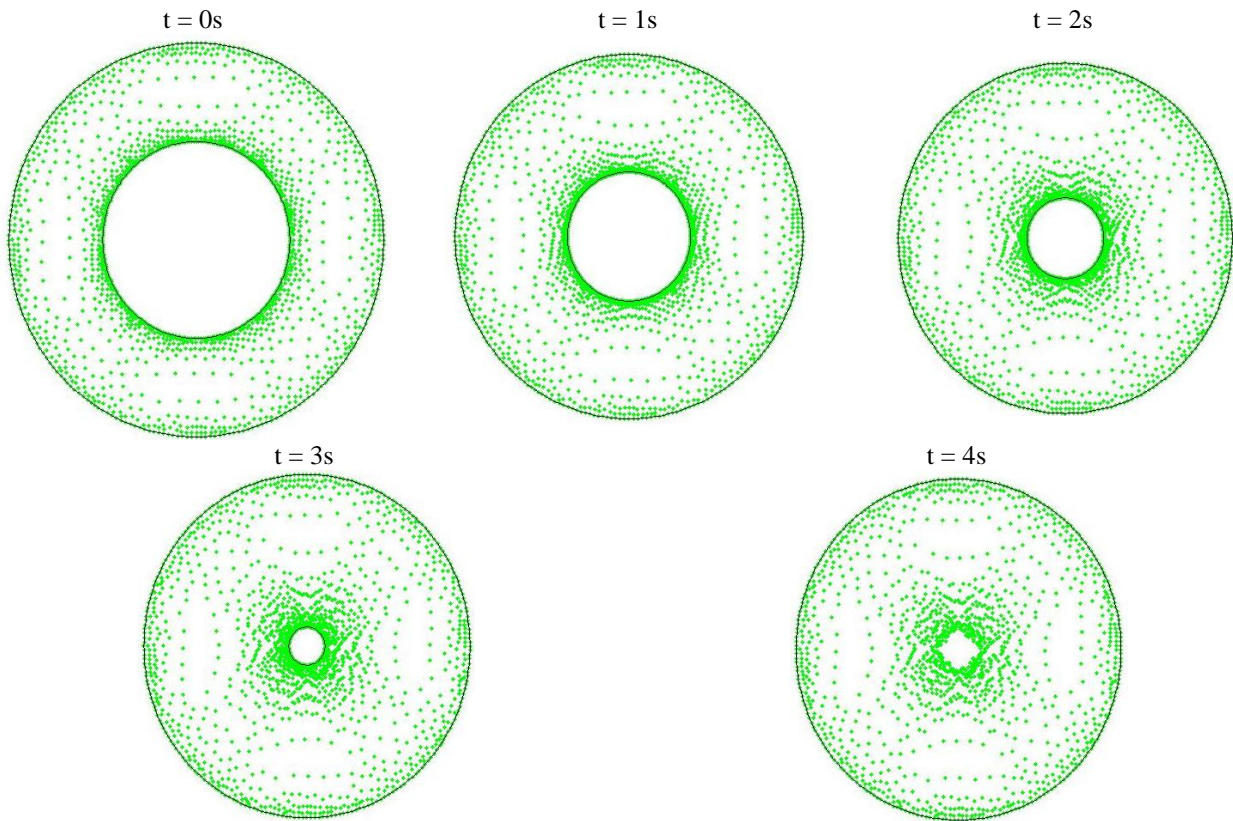

Figure 8 Initial simulation domain

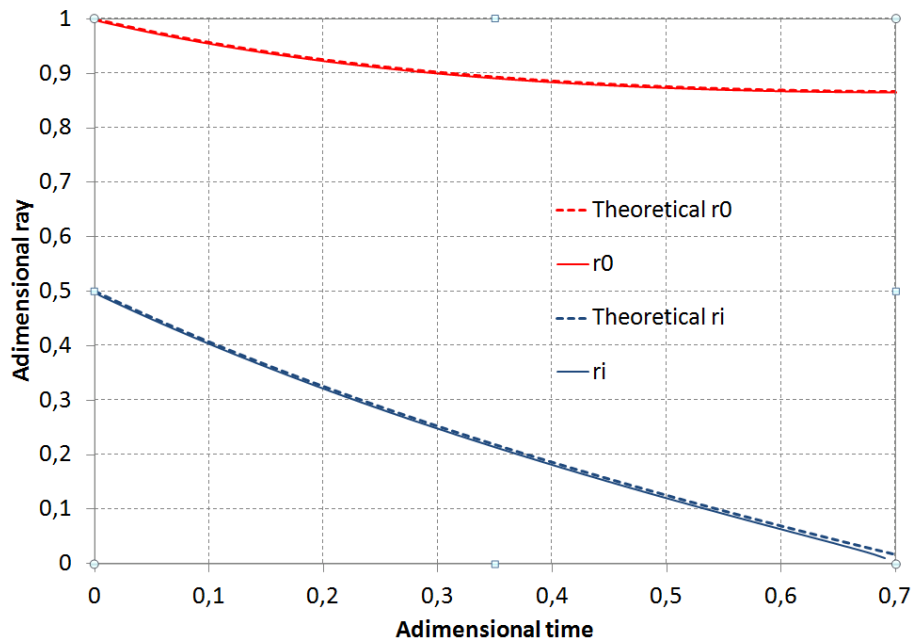The time evolution of internal and external rays r_i & r_0 is compared with the theory (Fig.9).

Figure 9 Comparison of the simulation results with theory

A good agreement is founded. The hydrodynamic simulation is validated.

<u>Thermal validation</u>

The thermal calculation is validated simulating three simple tests. Simulations are compared with analytic solutions for a plane at initial temperature, setting firstly a boundary temperature condition on a side, secondly an air temperature condition. Finally, we simulate a laser pass and compare the temperature evolution with a commercial finite element code. The interaction between laser and polymer was determined by laser absorption measurements through powder and is modeled with a Beer-Lambert law.

RESULTS AND DISCUSSION

Introduction

A single Selective Laser Melting process simulation is presented. It allows understanding the phenomenon and their time scale acting in the process.

Material and process parameters

The material and process parameters are presented in table 1 and 2. The parameters used are the one found in the literature for the melting of polymers like PEEK (Polyetheretherketone). The initial mesh has been obtained using images realized by X-ray micro tomography on a PEEK powder. The studied area is a square which side is 500µm.

Table 1 – Material parameters.

Surface tension	30 mN.m^{-1}
Conductivity	0.25 W.m^{-1}.K^{-1}
Heat capacity	1320 J.Kg^{-1}K^{-1}
Air/Polymer convection coefficient	15 W.m^{-2}.K^{-1}
Melting Temp.	Tm = 340°C
Crystallization Temp.	300°C
Viscosity	$\eta(T) = 810e^{\frac{82200}{R}\left(\frac{1}{T}-\frac{1}{Tm}\right)}$
Polymer density	1300 Kg.m^{-3}
Laser reflectivity	16%
Laser absorption coefficient	20000 m^{-1}

Table 2 – Process parameters.

Pre-heating temperature	310 °C
Air temperature	50 °C
Laser power	5W
Laser speed	0.5 m.s^{-1}
Laser beam diameter	300 µm

Simulation images

The initial domain is at the pre-heating temperature (Fig.10).
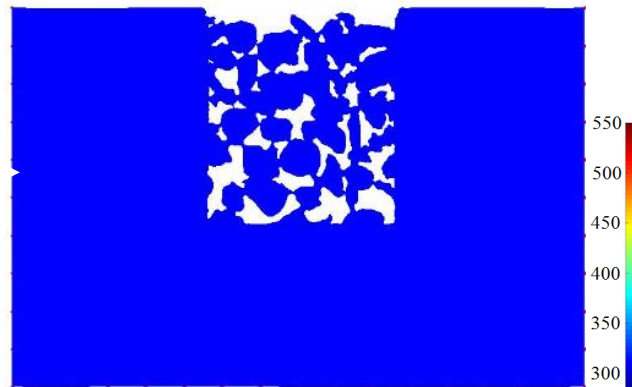

Figure 10 Initial domain pre-heated

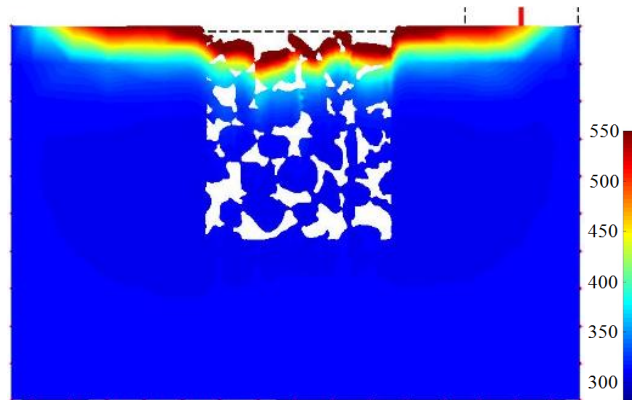The laser pass occurs during about 10 ms from left to right (Fig.11)

Figure 11 End of laser pass

The maximal temperature obtained after laser pass is 665°C. The material cools down extremely rapidly (Fig.12)
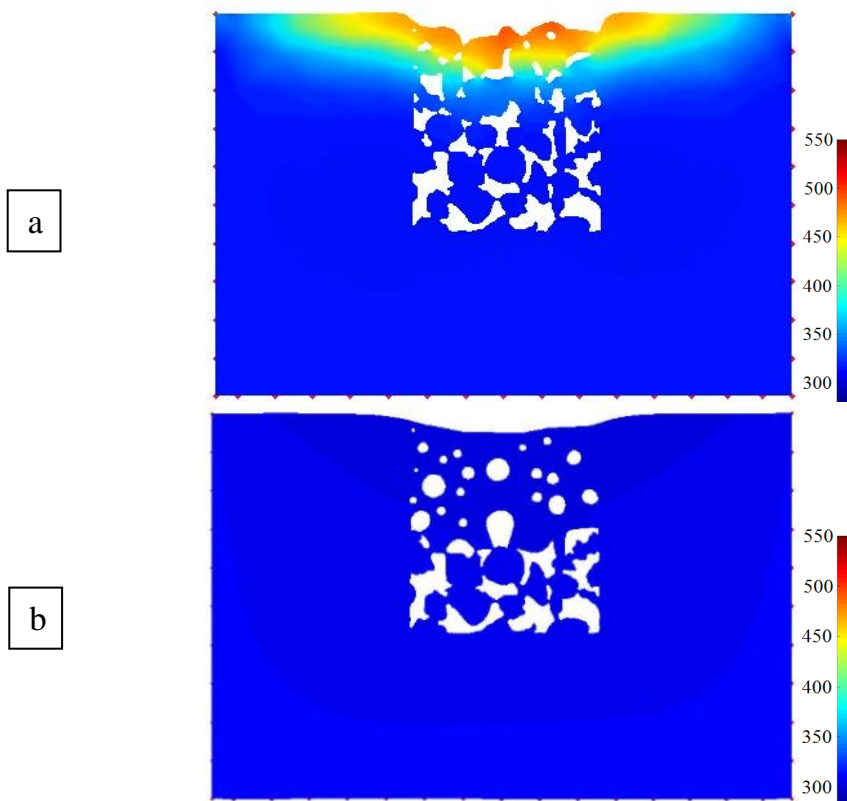

a

b

Figure 12 Material cooling
a) 21 ms after laser pass – b) 3 s after laser pass

Simulation results

This simulation enables to understand the characteristic times of each phenomenon during the process and evaluate the welding of the material.
The interface curvature adimensioned by its initial curvature evolution is presented (Fig.13). The evolution is very fast. In less than a second, coalescence of grains is much advanced.
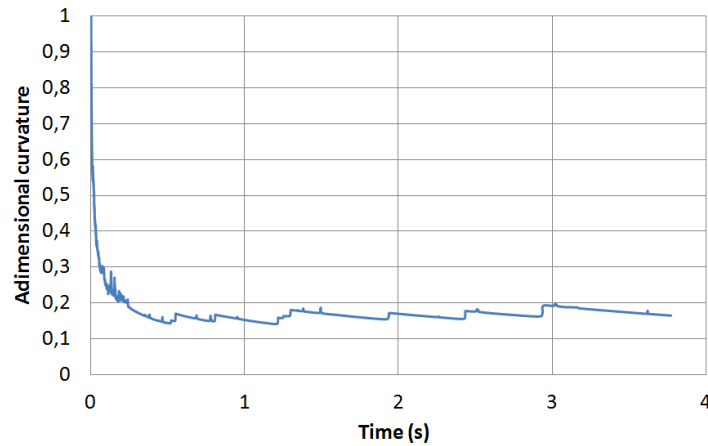

Figure 13 Interface curvature evolution

The welding of the material is also extremely rapid. Quite all the material melted has had enough time to get a good welding state. The good welded area is presented (Fig.14) 3 seconds after laser pass. A value of 1 represents a good welding.
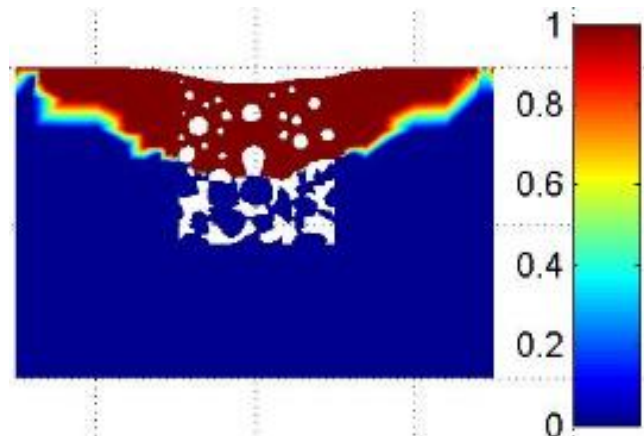

Figure 14 Welding state of the material 3 seconds after laser pass

A good welding depth is obtained until 370 µm. It corresponds quite well to experimental results. A good welding state has been obtained 84ms after the laser pass. Polymer has been melted until a depth of 385µm.
The evolution of the welding depth with time is presented (Fig.15). This curve is dependent on the nodes position.
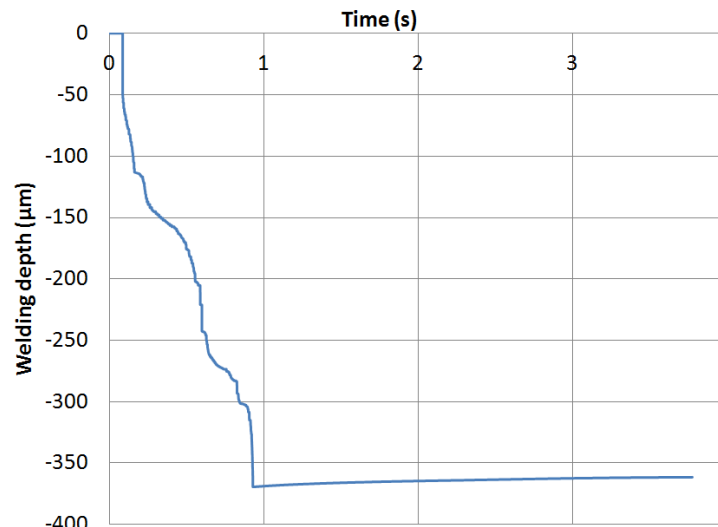
Figure 15 Welding depth evolution

After one second, the maximal welding depth is obtained.
In this situation, the melted polymer stays in a liquid state after the laser pass when the temperature has reached the initial temperature of the powder bed.

CONCLUSIONS

The process simulation has been performed in two dimensions. A lot of numerical difficulties (time step calculation and interface remeshing particularly) have been solved to be able to enable the calculation. These difficulties would be much more complicated to solve in 3D. Results in 2D are a first approach of the process.
The coalescence of grains is a rapid phenomenon taking place in some seconds, as well as the welding of the material. As coalescence phenomenon is fast, porosities should disappear rapidly. The presence of porosities in real parts can be explained by the apparition of closed ones. Then, their volume decreases with time through an air diffusion phenomenon. This phenomenon cannot be prompt in a bi-dimensional simulation.
Further work has to be done to compare experimental data and simulations, in order to confirm the correlation of the simulation with reality.
Future work will be done to compare different material and process parameters effects on the process, their effect on interface curvature and welding evolution particularly.
It will be also possible to determine the conditions inducing the solidification of the melted polymer, situation not suitable as the polymer has to stay melted as long as possible in order to increase density (air diffusion) and to reduce parts distortions.

Acknowledgements

References

1. R. Goodridge; C. Tuck; R. Hague *J. Progress in Materials Science* 2012**, 57,** 229.
2. D. Defauchy; G. Regnier; P. Peyre; I. Amran; A. Ammar in PPS 27 proceedings, Marrakech, 2011.
3. S. Dupin, PhD Thesis, INSA de Lyon, 2012.
4. G. Salmoria; J. Leite; R. Paggi *Polymer Testing* 2009**, 28-7,** 746.
5. D. Leigh in Additive Manufacturing International Conference, 2010.
6. J. Yvonnet, D. Ryckelynck, P. Lorong, F. Chinesta *International Journal for Numerical Methods in Engineering* 2004*, 60,* 1451.
7. Alfaro I., Yvonnet J., Chinesta F., Cueto E. *International Journal for Numerical Methods in Engineering 2007, 71, 1436.*
8. D. Defauchy; G. Regnier; I. Amran; P. Peyre; A. Ammar; F.Chinesta in COMPLAS XI proceedings, Barcelone, 2011.
9. C. Nicodeau, PhD Thesis, PIMM, 2005.
10. M.C.A. Kropinski; *Journal of Computational Physics*, 2002, *180*, 1-24